This document was prepared in conjunction with work accomplished under Contract No. DE-AC09-96SR18500 with the U. S. Department of Energy.

DISCLAIMER

WSRC-TR-2005-00477

TRANSMISSION ELECTRON MICROSCOPY STUDY OF HELIUM-BEARING FUSION WELDS (U)

By:

M. H. Tosten
M. J. Morgan

November 2005

Washington Savannah River Company
Savannah River Site
Aiken, South Carolina 29808

Prepared for the U.S. Department of Energy
Under Contract DE-AC09-96SR18500

SRNL
SAVANNAH RIVER NATIONAL LABORATORY

DISCLAIMER

Printed in the United States of America

Prepared For
U.S. Department of Energy

WSRC-TR-2005-00477

MS&T
MATERIALS SCIENCE AND TECHNOLOGY

Keywords: Helium Embrittlement
Stainless Steel
Fusion Welds

Retention: Permanent

TRANSMISSION ELECTRON MICROSCOPY STUDY OF HELIUM-BEARING FUSION WELDS (U)

By:

M. H. Tosten
M. J. Morgan

November 2005

Scott L. West
Authorized Derivative Classifier
S. L. West

12/12/2005
Date

Washington Savannah River Company
Savannah River Site
Aiken, South Carolina 29808

Prepared for the U.S. Department of Energy
Under Contract DE-AC09-96SR18500

SRNL
SAVANNAH RIVER NATIONAL LABORATORY

DOCUMENT: WSRC-TR-2005-00477

TITLE: TRANSMISSION ELECTRON MICROSCOPY STUDY OF HELIUM-BEARING FUSION WELDS (U)

APPROVALS

M. H. Tosten, Author
Materials Science and Technology

DATE: 12/12/2005

M. J. Morgan., Author
Materials Science and Technology

DATE: 12/14/2005

E. A. Clark, Technical Reviewer
Materials Science and Technology

DATE: 15 December 2005

J. S. Hölder, Customer
Hydrogen Technology

DATE: 12/15/2005

S. L. West, Manager
Materials Science and Technology

DATE: 12/12/2005

N. C. Iyer, Director
Materials Science and Technology

DATE: 12/12/2005

TRANSMISSION ELECTRON MICROSCOPY STUDY OF HELIUM-BEARING FUSION WELDS (U)

By:

M. H. Tosten
M. J. Morgan

Washington Savannah River Company
Savannah River National Laboratory
Aiken, SC 29808

ABSTRACT

A transmission electron microscopy (TEM) study was conducted to characterize the helium bubble distributions in tritium-charged-and-aged 304L and 21Cr-6Ni-9Mn stainless steel fusion welds containing approximately 150 appm helium-3. TEM foils were prepared from C-shaped fracture toughness test specimens containing delta (δ) ferrite levels ranging from 4 to 33 volume percent. The weld microstructures in the low ferrite welds consisted mostly of austenite and discontinuous, skeletal δ ferrite. In welds with higher levels of δ ferrite, the ferrite was more continuous and, in some areas of the 33 volume percent sample, was the matrix/majority phase. The helium bubble microstructures observed were similar in all samples. Bubbles were found in the austenite but not in the δ ferrite. In the austenite, bubbles had nucleated homogeneously in the grain interiors and heterogeneously on dislocations. Bubbles were not found on any austenite/austenite grain boundaries or at the austenite/δ ferrite interphase interfaces. Bubbles were not observed in the δ ferrite because of the combined effects of the low solubility and rapid diffusion of tritium through the δ ferrite which limited the amount of helium present to form bubbles and/or the limited resolution of TEM technique used to image the bubbles.

TABLE OF CONTENTS

Page No.

BACKGROUND

Over the years, research studies at the SRS have focused on the effects of tritium and its decay product, helium-3, on the mechanical properties of austenitic stainless steels used to contain tritium gas (e.g., Ref. 1-3). These studies have shown that the presence of tritium and helium-3 have a detrimental effect on the fracture toughness properties of these materials. Until recently, studies have focused mainly on the mechanical property variations that occur in the austenitic base materials. However, little work has been done to understand how tritium and helium-3 affect the mechanical properties of the fusion welds that are inherent to the design of some tritium storage vessels.

Typical fusion welds contain austenite (fcc phase) and a smaller amount of δ ferrite (bcc phase). The δ ferrite phase is needed to prevent solidification and liquation cracking when welding austenitic stainless steels. A recent study of tritium-free material showed that the microstructures that developed in multi-pass fusion welds are very complex and become increasingly so as the δ ferrite content increases (Ref. 4). Of prime interest in tritium/helium-containing welds is the role that δ ferrite plays in the deformation/fracture process and how the presence of this phase affects the helium bubble microstructure in the fusion zones.

The purpose of this study was to document the helium bubble distribution that existed in fusion welds made on 304L and 21Cr-6Ni-9Mn stainless steels. This study provided a foundation for understanding the influence of weld microstructure on the helium bubble distribution (size and location) in both the heat-affected zones (HAZs) and fusion zones of these welds.

EXPERIMENTAL PROCEDURE

A series of tritium-charged-and-aged fusion welds, with a range of δ ferrite contents, were prepared using 304L and 21Cr-6Ni-9Mn stainless steel base materials in combination with electron beam (EB) welding and a variety of stainless steel filler wires. The base materials were a 304L weld critical (WC) plate, a 304L and a 21Cr-6Ni-9Mn cylindrical forging. The 304L forging was prepared by a high-energy-rate-forging (HERF) process while the 21Cr-6Ni-9Mn forging was fabricated using a convention forging process. Ferrite levels in the welds varied from about 4 vol.% (EB weld on 304L WC plate) to 33 vol.%. The higher ferrite welds were made using Type 308L, 309L MOD (modified for higher ferrite content), and 312 MOD stainless steel filler wires. The chemical compositions of the materials used in this study are shown in Table 1 and the welds prepared for analysis are listed in Table 2.

Once welded, the base materials were sectioned into C-shaped fracture toughness specimens (see Figure 1). These specimens were exposed to tritium gas at a temperature of 350°C and a pressure of about 5000 psi for 3 weeks. The conditions of the charging were designed to saturate the samples with tritium without changing the starting microstructure. After charging, samples were aged for 8 months at -23°C to produce a helium content of ~150 appm. Measured helium concentrations in the base metals agreed well with the calculated, target helium concentrations; however, weldments had 33-50% less helium than expected (see Table 3).

Specimens for TEM analysis were prepared from C-shaped specimens after fracture toughness testing. Figure 2 is a schematic illustration of the sample sectioning procedure. Several thin slices were cut from each test specimen beginning immediately adjacent to the fracture surface (plastically deformed region) and continuing into the weld heat-affected zone and base metal. Two 3 mm diameter disks were punched from each slice. Thin foils were prepared from each disk using a twin jet electropolisher and a solution of 57% methanol, 39% butyl cellosolve, and 4% perchloric acid at 35Vdc and 243 K. All TEM was performed using a JEOL 2010 microscope operating at 200 kV.

RESULTS

General Microstructure

Welds with a range of δ ferrite contents of 4 to 33 vol.% were examined in this study. Images shown in Figures 3a-d illustrate the variety of microstructures observed in the weld fusion zones. Figures 3a-c show the morphological differences in the δ ferrite phase as the volume fraction and Cr_{eq}/Ni_{eq} ratio in the weldments increased (Cr_{eq} = %Cr + %Mo + 0.7%Nb (ferrite stabilizers) and Ni_{eq} = %Ni + 35%C + 20%N + 0.25%Cu (austenite stabilizers)). The microstructure of the weld made using the 304L HERF forging and 308L filler wire (i.e., the 48 weld) is shown in Figure 3a. The average ferrite content of this weld was about 8 vol.% (Cr_{eq}/Ni_{eq} ratio of ~1.65). The microstructure shown in this image was also typical of the EB and 98 welds that were examined and consisted of discontinuous, skeletal ferrite in an austenite matrix. (The constituent phases were identified using selected area electron diffraction.) Skeletal ferrite (or retained ferrite) is ferrite located at the cores of the original, primary δ ferrite dendrites that did not transform to austenite upon cooling.

Figure 3b is an image from the 8309 weld (304L WC plate + mixture of 308L and 309L MOD wires). This weld contained approximately 12 vol.% δ ferrite on average (Cr_{eq}/Ni_{eq} ratio of ~1.85). The δ ferrite in this weld formed as a continuous network around the austenite grains. Additionally, the ferrite/austenite boundaries were more planar in this weld when compared to the more rounded interfaces observed in Figure 3a. Welds made with the 309L MOD and 312 MOD wires also contained a large number of oxide inclusions (e.g., at arrow in Figure 3b). X-ray analysis showed that these particles were enriched in Mn, Cr, Ti, S, Al. (and O) when compared to the austenite matrix, and are believed to have originated from oxide impurities associated with the modified weld wires.

The weld containing the most δ ferrite (about 33 vol.%, Cr_{eq}/Ni_{eq} ratio ~2.33) was made using 309L MOD filler wire on the 304L HERF forging (i.e., weld "49"). The microstructure in many regions of this weld looked very similar to that seen in Figure 3b. In other areas the morphologies of the δ ferrite and austenite were very different as seen in Figure 3c. In this image the δ ferrite is the continuous phase and "surrounds" a large number of small, irregularly-shaped austenite grains. This type of microstructure is more prevalent in the higher Cr_{eq}/Ni_{eq} ratios welds which solidify at single phase ferrite and subsequently transform to austenite by a nucleation and growth mechanism. The planar austenite/ferrite interfaces observed in this image are indicative of a microstructure that formed via this mechanism.

Figure 3d is an image from a region of the "48" weld that was located close to the fracture surface of a C-shaped test specimen. This image shows a microstructure that is mostly austenite with some skeletal ferrite. The more distinctive features in this image, however, are the deformation twins (e.g., marked with arrows) in the austenite. Plastic deformation by way of twinning was observed in all welds in regions closest to the fracture surfaces of the test specimens. Delta ferrite appeared to provide some resistance to deformation, particularly in specimens with higher Cr_{eq}/Ni_{eq} ratios.

Helium-Bearing Welds

In general, the helium bubble distribution in all welds was very similar. Specifically, helium bubbles were observed in the austenite but not in the δ ferrite. Figure 4 is an image from a weld made on the 21Cr-6Ni-9Mn conventional forging using 308L filler wire. This image shows a δ ferrite "grain" in an austenite matrix. The small black "dots" visible in the austenite matrix arise from strain contrast associated with the presence of helium bubbles. As evidenced in Figure 4, black "dots" (bubbles) are not present in the δ ferrite. Careful examination of many δ ferrite regions under a variety of tilt/contrast conditions failed to locate any bubbles in the δ ferrite phase in any of the welds.

The distribution of helium bubbles in the austenite in all of the weldments closely matched the helium bubble microstructure observed in the weld HAZs. That is, helium bubbles were observed within the grain interiors and not on the grain boundaries. The helium bubble distribution in the austenite is illustrated in Figure 5. These images are from austenite regions in a mixed wire weld on the 304L plate. Figure 5a is a high magnification image showing bubbles that nucleated in the interior of an austenite grain. The imaging conditions were such that many 2-3 nm sized bubbles (appearing as small "white" dots in this under-focused image) were visible. These bubbles likely formed by "homogeneous" nucleation at vacancies or vacancy clusters which are strong traps for helium in the matrix. In other austenite grains, helium bubbles were observed on dislocations (Figure 5b). Dislocations are known to be potent heterogeneous nucleation sites for bubbles (Ref. 5,6).

Interfaces play an important roll in the fracture processes in tritium/helium-containing materials, so the austenite/austenite and austenite/δ ferrite boundaries in the weldments were investigated carefully. A typical interphase boundary is imaged in Figure 6. Close examination of this and many other interfaces failed to detect bubbles at these locations. As mentioned above, the black "dots" in the austenite grain indicate the locations of helium bubbles. Again, there are no black "dots" in the δ ferrite region in this image. Examination of the near-boundary region in this image also revealed a narrow region extending along the boundary region that is devoid of bubbles. Regions like this are termed bubble-free zones (BFZs) and were observed previously in another study (Ref. 7). BFZ formation is believed related to the reduction in the vacancy concentration in the near-boundary region which reduces the amount of trapped helium available to form bubbles. In general, the helium bubble microstructures observed in the austenite within the weld metal were completely consistent with the microstructures observed in previous studies of tritium-charged-and-aged stainless steels.

DISCUSSION

The helium bubble distributions observed in the austenite phase were consistent with those observed in other studies at SRNL (Ref. 1,3-5,7). In these studies, helium bubbles were observed commonly in the grain interiors, on dislocations, and sometimes on carbide/matrix interfaces and austenite/austenite grain boundaries. In the present study, helium bubbles were not observed in the δ ferrite phase. There are at least two possible reasons for this. Firstly, it may simply be that there is less helium present in the δ ferrite to form bubbles. Unlike the fcc austenite phase (high hydrogen/tritium solubility and low diffusivity), the bcc ferrite phase is characterized by low hydrogen solubility and the rapid diffusion of hydrogen through the metal lattice. Therefore, the ferrite lattice tends to reject hydrogen and what is there diffuses out more rapidly before it decays to helium-3. Calculations show that pure α ferrite (also bcc) charged and aged using the sample conditions employed in the current study would contain about 13 appm helium (Ref. 8). This value is about 10 times less than the measured helium concentrations in the fully austenitic base materials (see Table 3). (Diffusivity/solubility differences may also explain the variability in the measured helium content of the welds as well as the drop-off in helium content in those welds containing high levels of ferrite.) As a result, the helium in the ferrite may be more widely dispersed over a large number of trap sites thus reducing the available helium in any one area to form a stable cluster or, at least, a cluster large enough to view in the TEM.

The second reason for not seeing helium bubbles in the δ ferrite may be related to the technique used to image them. Nanometer-sized helium bubbles are imaged in the TEM using an under/over-focusing technique (Ref. 9). In the under-focused condition bubbles appear brighter than the background, i.e., they look like voids, and in the over-focused condition bubbles appear as black dots and are darker imaging than the background. This imaging technique, however, is limited to resolving bubbles greater than about 0.7 nm in diameter. Below this size bubbles cannot be discerned from the background contrast in the image. Therefore, as alluded to above, bubbles (or maybe in fact, clusters of helium atoms) could have been present in the δ ferrite but were too small to be resolved in the TEM images.

SUMMARY

The helium bubble distributions in fusion welds containing 4 to 33 volume percent δ ferrite and approximately 150 appm helium-3 were characterized. In the low δ ferrite welds, the microstructure was primarily austenite and discontinuous, skeletal δ ferrite. In welds with higher levels of δ ferrite levels, the ferrite was more continuous and the austenite/ferrite interfaces more planar. In some areas of the highest δ ferrite weld, the ferrite was the matrix phase. Helium bubbles were observed in the austenite phase and not in the δ ferrite. The failure to observe bubbles in the δ ferrite was probably related to the limited solubility and the rapid diffusion of tritium in that phase resulting in a reduced amount of helium available to form bubbles of sufficient size to view in the TEM. Bubbles in the austenite nucleated homogeneously in the grain interiors and on matrix dislocations. These results were consistent with previous studies of helium bubbles in austenitic stainless steels. Bubbles were not observed on the austenite/austenite or austenite/ferrite boundaries.

ACKNOWLEDGEMENTS

The authors would like to express their appreciation to S.L. West for his valuable technical input and to G. K. Chapman for preparing the weld test specimens.

REFERENCES

1) M. J. Morgan and M. H. Tosten, "Microstructure and Yield Strengths Effects on Hydrogen and Tritium-Exposed HERF Stainless Steels": in Hydrogen Effects on Material Behavior, Proc. 4th Int. Conf. on the Effects of Hydrogen on the Behavior of Materials, Jackson Lake Lodge, WY, N. R. Moody and A. W. Thompson, eds., TMS, Warrendale, PA, 1990, pp. 447-58.

2) M. J. Morgan and D. A. Lohmeier, "Threshold Stress Intensities and Crack Growth in Tritium-Exposed HERF Stainless Steels": in Hydrogen Effects on Material Behavior, Proc. 4th Int. Conf. on the Effects of Hydrogen on the Behavior of Materials, Jackson Lake Lodge, WY, N. R. Moody and A. W. Thompson, eds., TMS, Warrendale, PA, 1990, pp. 459-68.

3) M. J. Morgan and M. H. Tosten, "Tritium and Decay Helium Effects on the Fracture Toughness Properties of Types 316L, 304L, 21Cr-6Ni-9Mn Stainless Steels": in Hydrogen Effects in Materials, Proc. 5th Int. Conf. on the Effects of Hydrogen on the Behavior of Materials, Jackson Lake Lodge, Moran, WY, N. R. Moody and A. W. Thompson, eds., TMS, Warrendale, PA, 1996, pp. 873-82.

4) M. H. Tosten and M. J. Morgan, "Microstructural Study of Fusion Welds in 304L and 21Cr-6Ni-9Mn Stainless Steels", WSRC-TR-2004-00456, Westinghouse Savannah River Company, Aiken, SC 29808.

5) M. H. Tosten and M. J. Morgan, "The Effects of Helium Bubble Microstructure on Ductility in Annealed and HERF 21Cr-6Ni-9Mn Stainless Steel", WSRC-RP-92-551, Westinghouse Savannah River Company, Aiken, SC 29808.

6) S. L. Robinson, "Tritium and Helium Effects on Plastic Deformation in AISI 316 Stainless Steel", Mater. Sci. Eng., 1987, vol. 96., pp. 7-16.

7) M. H. Tosten and P. A. Kestin, "Helium Bubble Distributions in Reactor Tank Repair Specimens - Part I.", WSRC-TR-91-141, Westinghouse Savannah River Company, Aiken, SC 29808

8) E. A. Clark, Unpublished calculations, Westinghouse Savannah River Company, Aiken, SC 29808.

9) M. F. Rhüle, "Transmission Electron Microscopy of Radiation-Induced Defects": in Radiation-Induced Voids in Metals, Proc. Int. Conf., June 1971, J. W. Corbett and L. C. Ianniello, eds., U.S. Atomic Energy Commission, 1972, pp. 255-91.

Table 1
Chemical Compositions of Materials

	304L HERF	21-6-9 CF	304L WC Plate[a]	308L Wire	309LM Wire[b]	312M Wire[b]
Cr	19.9	19.3	17.8	20.5	23.56	28.7
Ni	10.4	6.7	11.1	10.3	8.55	9.17
Mn	1.7	9.9	1.90	1.56	1.2	1.45
Mo	0.04	-	0.195	<0.01	2.5	0.27
C	0.029	0.031	-	0.028	0.02	0.05
Si	0.63	0.38	0.544	0.5	0.64	0.51
Cu	-	-	0.123	0.015	0.31	0.31
P	0.015	0.01	0.064	0.006	0.022	0.023
S	0.002	0.001	-	0.012	0.008	0.008
N	0.039	0.28	-	0.055	-	-
Co	0.03	-	0.065	0.068	-	-

[a]304L Plate, in-house Inductively Coupled Plasma Emission Spectroscopy results
[b]Manufactured as 309L and 316 metal sheath with powder metal core

Table 2
Fusion Weld Matrix

Sample ID	Base Metal[a]	Filler	Vol.% Ferrite[b]	Cr_{eq}/Ni_{eq}[c]
EB	304L (WC Plate)	EB Weld	4	1.62
98	21-6-9 (CF)	308L	5	1.58
48	304L (HERF)	308L	8	1.65
8309	304L (WC Plate)	308L/309L MOD Mix	12	1.85
8312	304L (WC Plate)	308L/312 MOD Mix		1.85
912	21-6-9 (CF)	312 MOD	24	2.17
412	304L (HERF)	312 MOD	24	2.27
49	304L (HERF)	309L MOD	33	2.33

[a]WC - weld critical, HERF - high energy rate forged, CF - conventionally forged
[b]Average ferrite content measured at center of notch
[c]Based on Table 2 compositions, 35% dilution of the weld by the base metal, and the WRC-1992 Cr and Ni equivalency equations:

$$Cr_{eq} = Cr + Mo + 0.7\ Nb,\ Ni_{eq} = Ni + 35C + 20\ N + 0.25\ Cu$$

Table 3
Helium Concentration of Weldments[a]

Sample No.	Mass[b] (mg)	Measured ^{3}He (10^{15} atoms)	Helium Concentration (appm)[c] Measured	Average[d]
EB	3.168	2.690	77.90	86.0
	5.784	5.933	94.11	±11.5
98	1.736	2.287	120.9	123
	3.773	5.147	125.2	±3
8309	1.130	0.9872	80.15	88.7
	4.296	4.554	97.25	±12.1
8312	2.832	2.429	78.69	84.3
	3.227	3.162	89.90	±7.9
912	3.758	4.475	109.2	111
	4.065	4.981	112.4	±2
412	1.486	1.053	65.01	71.3
	2.934	2.483	77.64	±8.9
49	3.313	1.602	44.36	51.9
	3.893	2.522	59.43	±10.7
304L BASE METAL	2.333	3.400	133.7	129
	4.293	5.774	123.4	±7
21-6-9 BASE METAL	1.805	3.953	200.9	161
	5.389	7.115	121.1	±56

[a]Sample 48 was not analyzed for helium content.

[b]Mass of specimen for analysis. Mass uncertainty is ±0.002 mg.

[c]Helium concentration in atomic parts per million (10^{-6} atom fraction) with respect to the total number of atoms in the specimen. Uncertainty is estimated to be ±1%.

[d]Mean and standard deviation (1σ) of duplicate analyses.

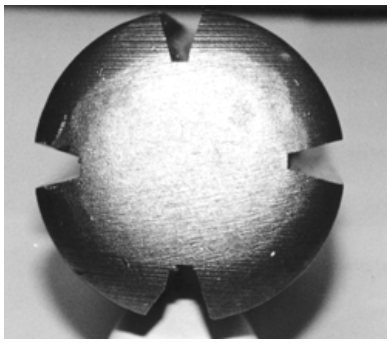

a

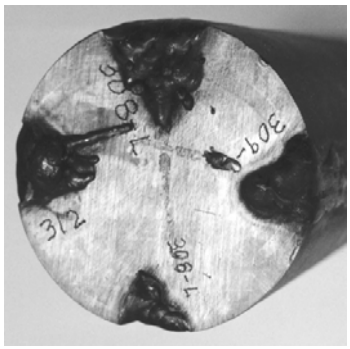

b

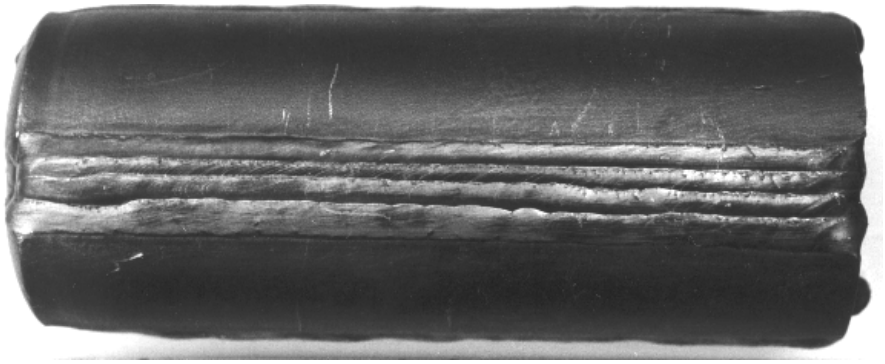

c

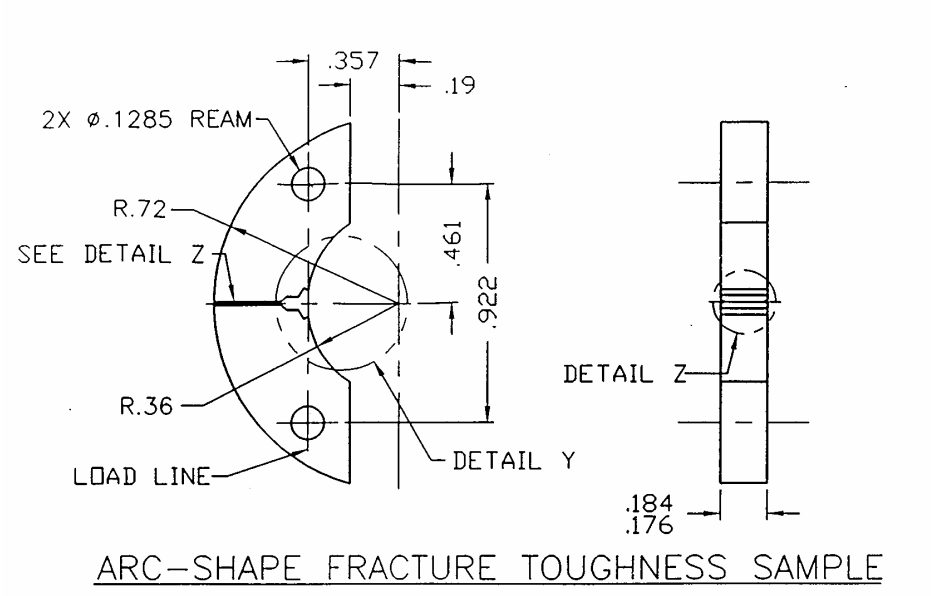

d

Figure 1. Images of a 3.125" dia. 304L HERF forging showing (a) the V-grooves prior to welding, (b) a cross-section of forging after welding, (c) one weld (showing multiple passes) along the 8" length of the same forging, and (d) a schematic of fracture toughness specimen machined from the forgings and weld critical plate. Specimens were machined so the notch would be located at the weld center line.

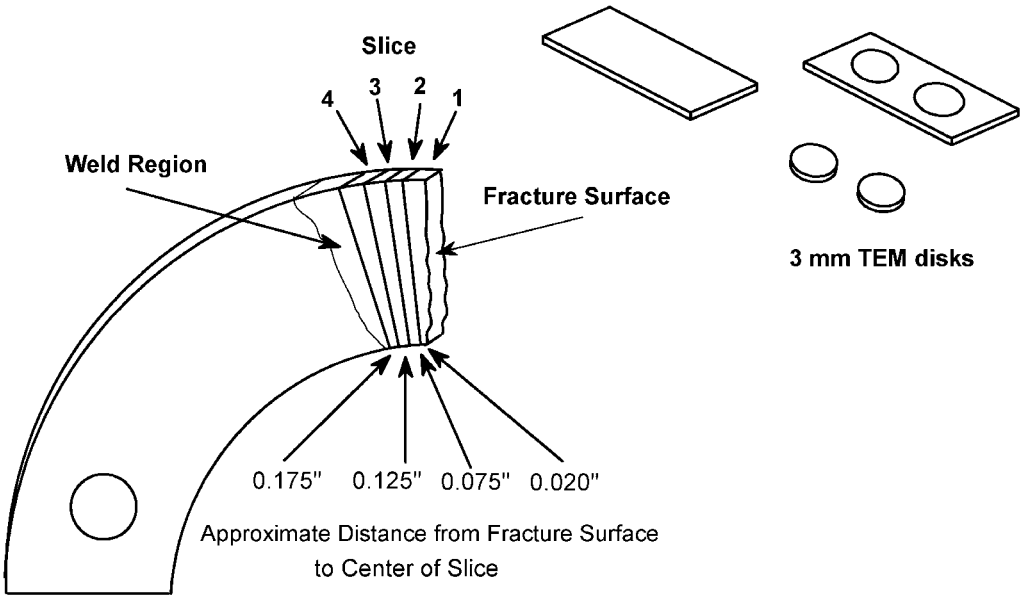

Figure 2. Schematic diagram illustrating the sectioning procedure used to generate TEM disks from the fusion weld region of a fracture toughness specimen. TEM samples were prepared from as close to the fracture surface as possible - potentially a plastically deformed region. Additional slices were sectioned from the weld and heat-affected zone.

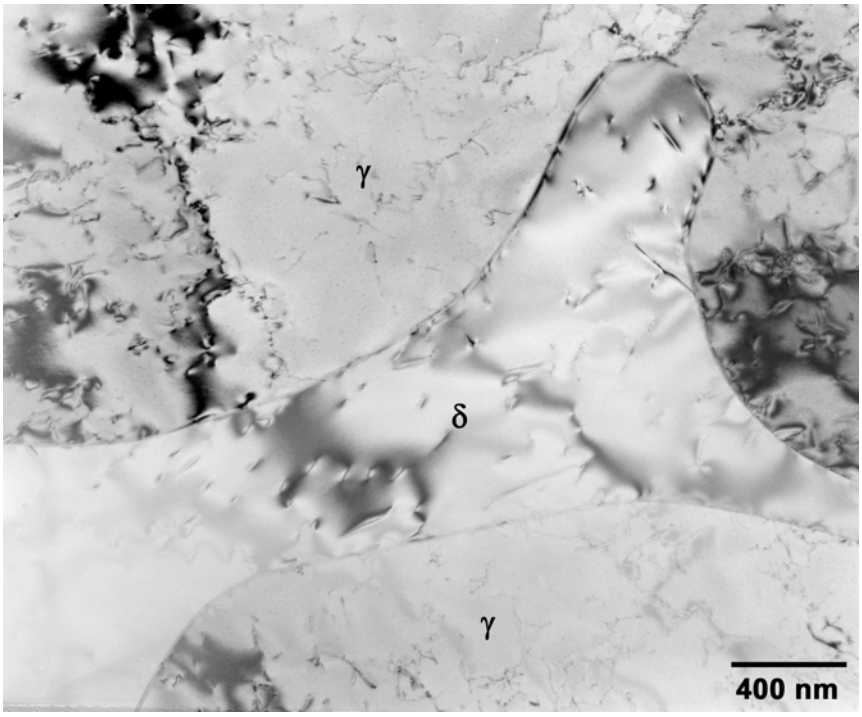

a

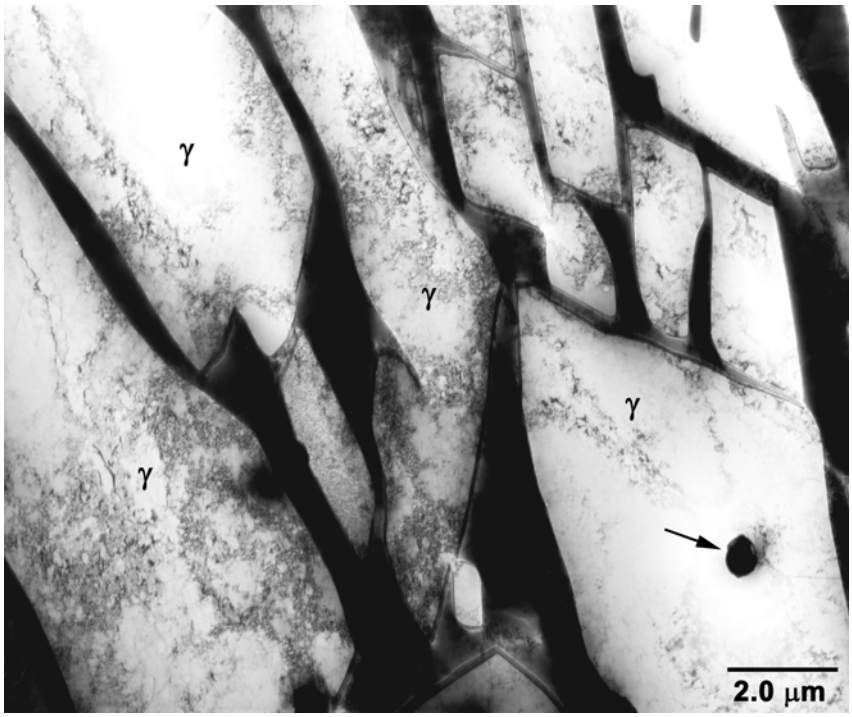

b

Figure 3. Images of weld microstructures observed in the (a) 48 weld (~8 vol.% δ ferrite), (b) 8309 weld (~12 vol.% δ ferrite), and (c) 49 weld (~33 vol.% δ ferrite). (d) Deformation twinning in the plastically deformed region of the 48 weld. Oxide inclusions are located at the arrow in (b) and at "A" in (d).

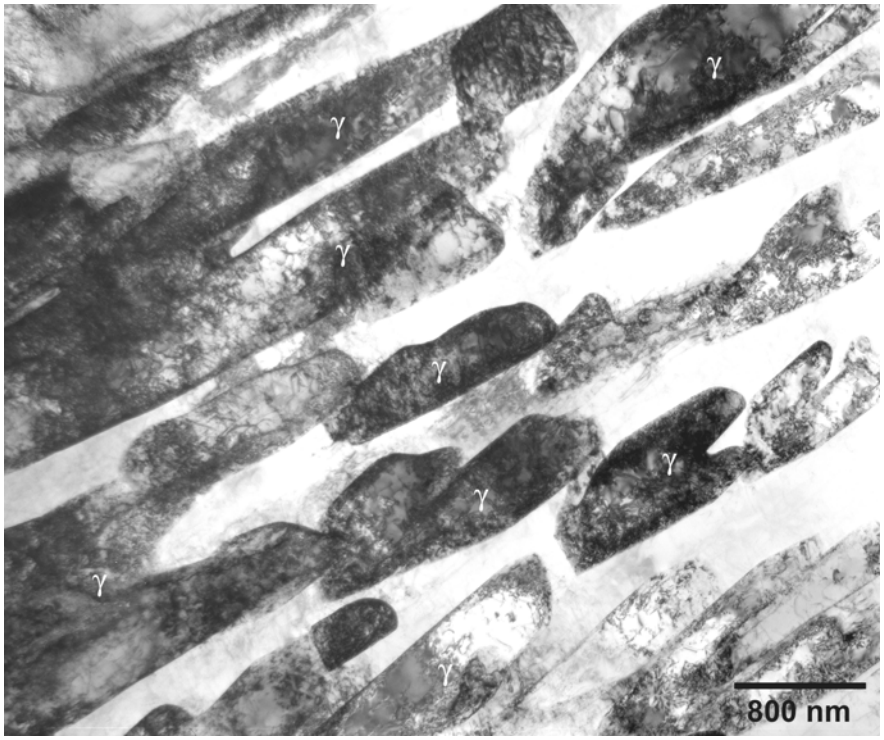

c

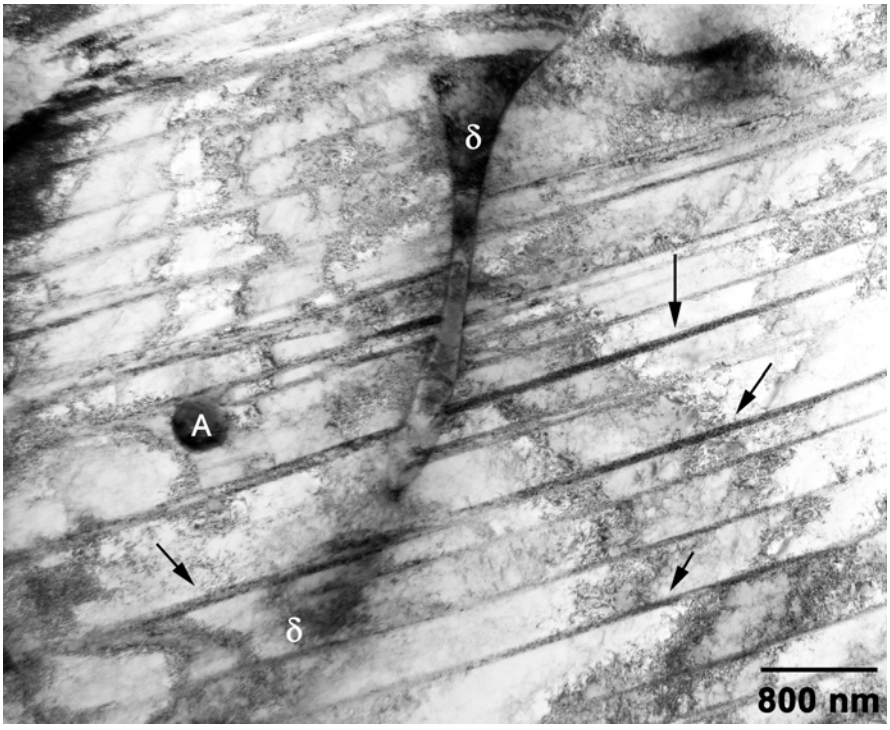

d

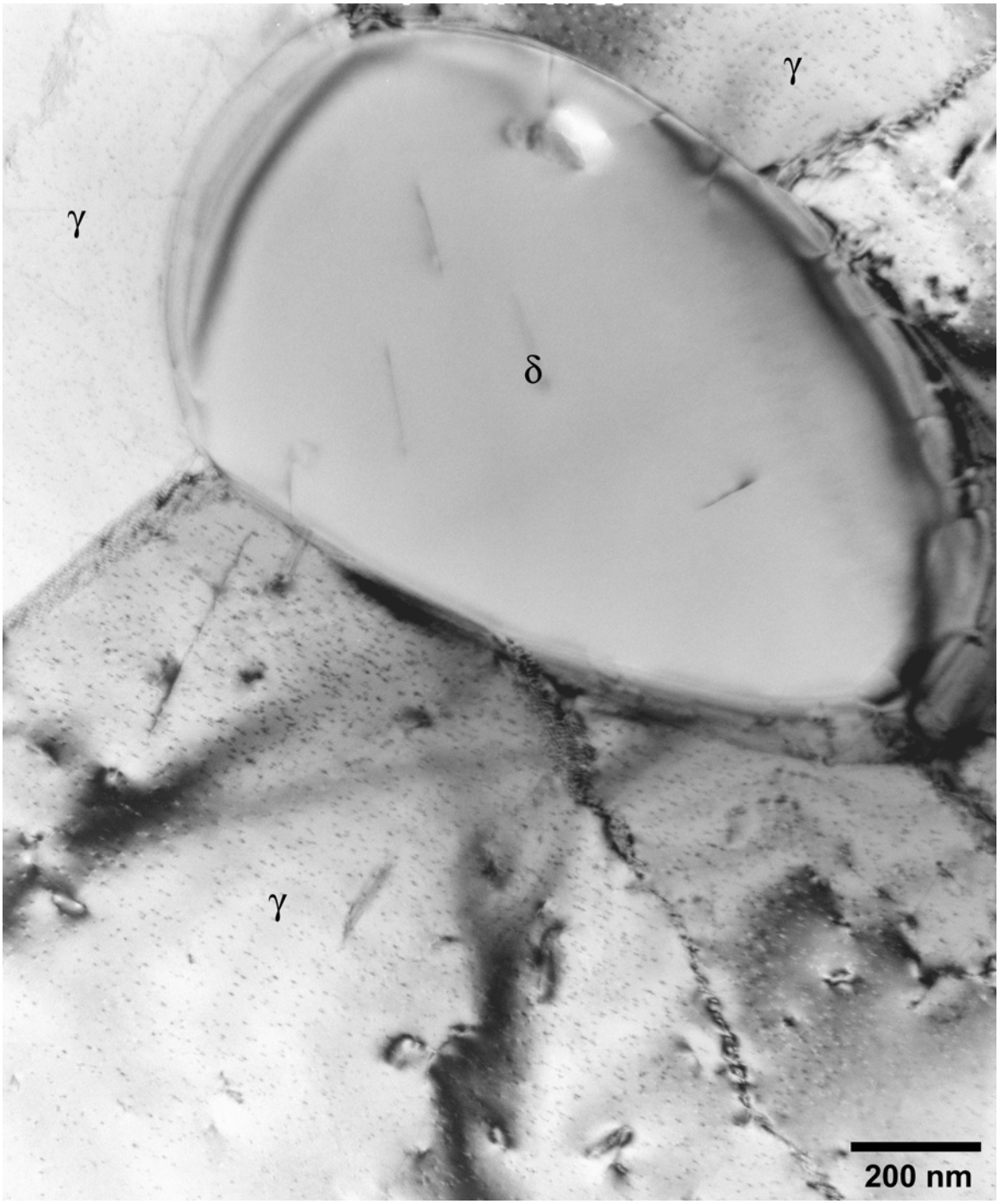

Figure 4. Image from the 98 weld (~5 vol.% δ ferrite) that shows a δ ferrite grain in an austenitic matrix. The black "dots" in the austenite arise from strain contrast from helium bubbles. No black "dots" are visible in the δ ferrite.

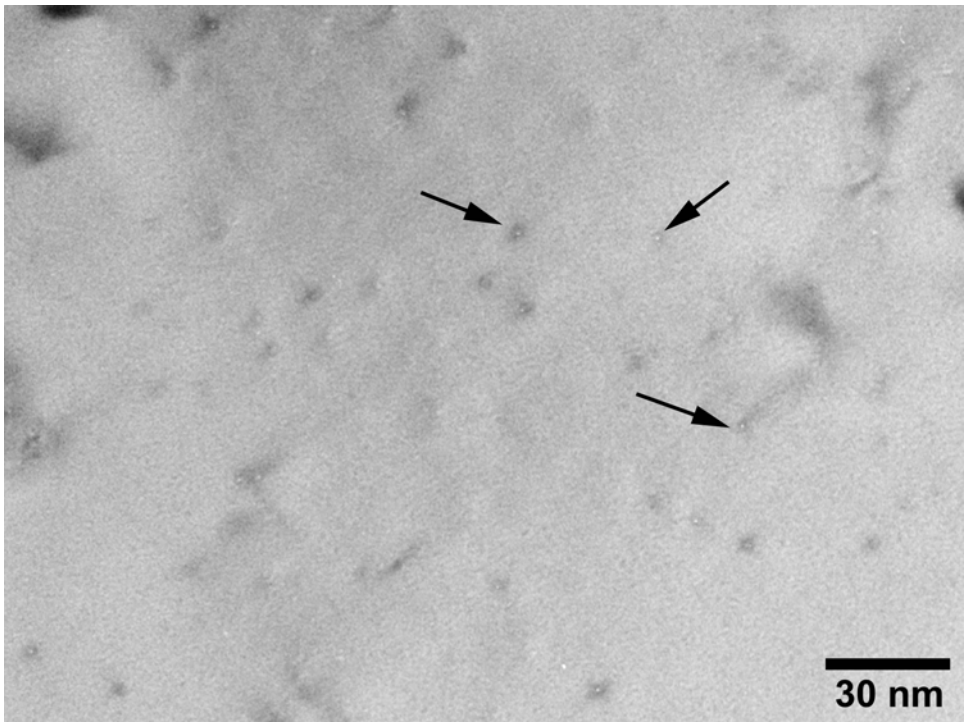

a

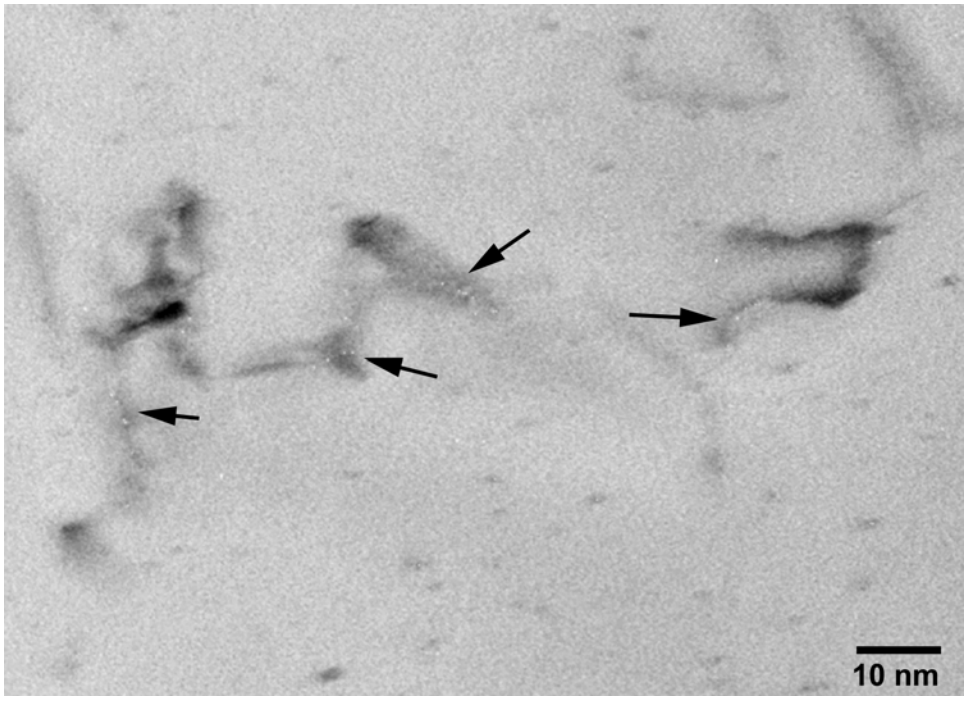

b

Figure 5. Helium bubbles in the austenite phase in the 8309 weld. Bubbles have formed in the matrix by homogeneous nucleation (a) and on dislocations in (b).

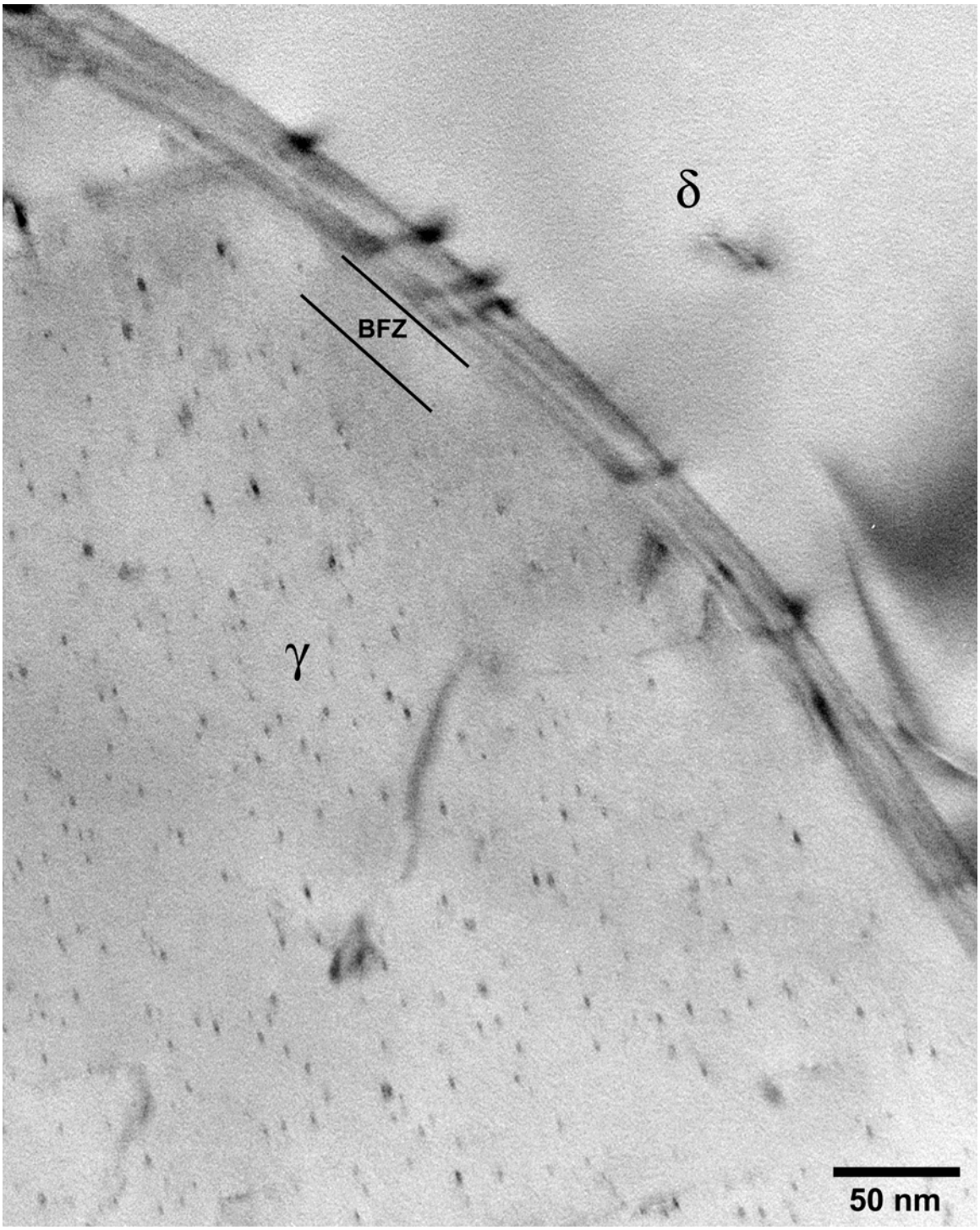

Figure 6. Image of an interface boundary between the austenite and the δ ferrite in the 48 weld. Bubbles were not observed on these type boundaries (or in the δ ferrite). A bubble-free zone exists in the near the boundary in this image.

DISTRIBUTION:

S. L. Robinson, Sandia/CA
B. P. Somerday, Sandia/CA
B. A. Meyer, LANL
D. A. Lohmeier, LANL
B. D. Wilkinson, LANL
P. E. Schembri, LANL

N. C. Iyer, 773-41A
P. F. Cloessner, 773-A
J. S. Hölder, 735-11A
S. B. Wyrick, 773-A
S. L. West, 773-A
E. A. Clark, 773-A
P. S. Korinko, 773-A
K. H. Subramanian, 773-A
G. K. Chapman, 773-A
E. J. Majzlik, 773-A
E. G. Caveness, 773-A
MTS File, 773-41A